Effect of Surface Cracks on Rayleigh Wave Propagation: An Experimental Study

A. Zerwer[1]; M. A. Polak[2]; and J. C. Santamarina[3]

Abstract: This experimental study investigates the use of Rayleigh waves for crack detection in structural elements. Receiver arrays measure surface accelerations at various locations with respect to a vertical slot cut into a thin Plexiglas sheet. Two-dimensional Fourier transform calculations provide Rayleigh wave dispersion and energy with respect to various slot depths. In addition, autospectrum calculations aid in defining slot location. It is shown that slots reflect short wavelengths and allow the transmission of long wavelengths. Slot location is easily identified from autospectrum measurements; however, accurate determination of slot depth is dependent on the aperture function of the array.

DOI: 10.1061/(ASCE)0733-9445(2002)128:2(240)

CE Database keywords: Cracking; Wave propagation; Rayleigh waves; Nondestructive evaluation.

Introduction

Cracks caused by applied mechanical loads, fatigue, shrinkage, or corrosion often form on free surfaces of structural elements. Such discontinuities affect structural integrity and performance. Proper assessment of surface anomalies is necessary for optimal decisions regarding rehabilitation, strengthening, and rebuilding existing structures. This paper presents an experimental study on Rayleigh wave propagation in structural elements. The aim of this study is to develop a nondestructive testing technique for detecting surface cracks in such elements.

While transillumination tomographic techniques can reveal internal defects, the reduced information content near free surfaces restricts their ability to detect surface features. On the other hand, surface information can be gathered with Rayleigh wave measurements. Rayleigh waves are ideally suited for this purpose because they are confined to the free surface of an object.

Several considerations must be taken into account when using Rayleigh waves for near-surface fracture detection. Of primary importance is the ratio of wavelength (λ) to fracture depth (d). Three regimes can be identified. When incident wavelengths are shorter than the fracture depth, $\lambda \ll d$, strongly reflected and weakly transmitted Rayleigh waves are generated. Equally strong transmitted and reflected Rayleigh wave energy exists when $\lambda \approx d$. Finally, incident wavelengths greater than fracture depth, $\lambda \gg d$, have weak reflection and strong transmission of Rayleigh wave energy, as the Rayleigh wave motion incorporates the slot as part of the material. Proper signal-processing techniques have been proposed for each λ/d regime (Victorov 1967; Woods 1968; Silk 1976; Domarkus 1978; Tittmann et al. 1978; Tittmann et al. 1980; Yew et al. 1984; Hirao et al. 1992).

The dimensions and geometry of the body subjected to Rayleigh wave probing must also be considered. In an infinite half-space, Rayleigh waves are formed by the interaction of body waves with a traction-free surface. The generation of Rayleigh waves in plates and beams is not as straightforward. As shown in Zerwer et al. (2000), Rayleigh waves in a plate are formed by the superposition of fundamental Lamb modes. The transition from fundamental mode behavior to Rayleigh wave motion is not distinct. This physical characteristic limits the penetration depth of a "pure" Rayleigh wave. In such cases, the ratio of wavelength to body dimensions (λ/h) becomes an important factor.

The methodology investigated in this study, for near-surface fracture detection using Rayleigh waves, involves broadband spectra. This allows sampling of both short and long wavelengths, thereby encompassing a wide range of λ/d and λ/h ratios. Rayleigh wave time history records are collected from a series of equidistant receivers forming a linear array. Subsequent data reduction entails calculating the two-dimensional Fourier transform of the receiver array and autospectral densities for each receiver measurement.

The experimental approach is similar to previous work done by Hévin et al. (1998), Pant and Greenhalgh (1989), and Yew et al. (1984). These studies measured Rayleigh wave attenuation with respect to fracture depth for receiver measurements made on either side of a fracture. Also, these studies use large plates to eliminate multiple reflections. The presented work differs from previous research by combining linear array techniques with autospectrum calculations to determine fracture location and depth. Array signal processing techniques allow the extraction of Rayleigh wave motion from measured time-domain traces that contain extraneous reflections. Experimental measurements are completed on specimens with realistic dimensions to include the effect of multiple reflections and to acknowledge the depth restriction of Rayleigh waves imposed by the finite dimensions of structural elements. Ultimately, the intention of this nondestruc-

[1]Research Associate, Dept. of Civil Engineering, Univ. of Waterloo, ON, Canada.

[2]Associate Professor, Dept. of Civil Engineering, Univ. of Waterloo, ON, Canada.

[3]Professor, Dept. of Civil and Environmental Engineering, Georgia Institute of Technology, Atlanta, GA.

Note. Associate Editor: Joseph W. Tedesco. Discussion open until July 1, 2002. Separate discussions must be submitted for individual papers. To extend the closing date by one month, a written request must be filed with the ASCE Managing Editor. The manuscript for this paper was submitted for review and possible publication on August 7, 2000; approved on August 13, 2001. This paper is part of the ***Journal of Structural Engineering***, Vol. 128, No. 2, February 1, 2002. ©ASCE, ISSN 0733-9445/2002/2-240–248/$8.00+$.50 per page.

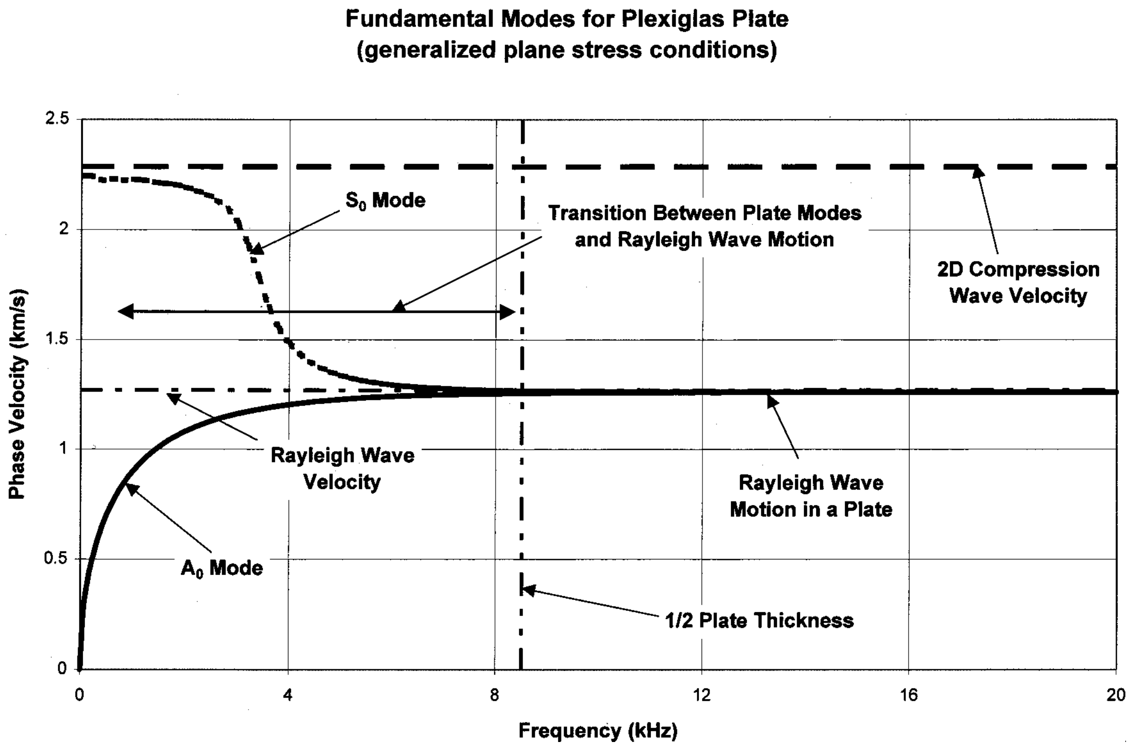

Fig. 1. Theoretical dispersion curves of fundamental Lamb modes in plate

tive testing approach is to detect and size fractures in structural elements of various geometries.

A brief review of fundamental concepts concerning steady-state wave propagation in thin plates follows. Then test configuration, signal processing, and results are presented in detail, followed by a discussion of the proposed methodology for detecting and sizing surface discontinuities.

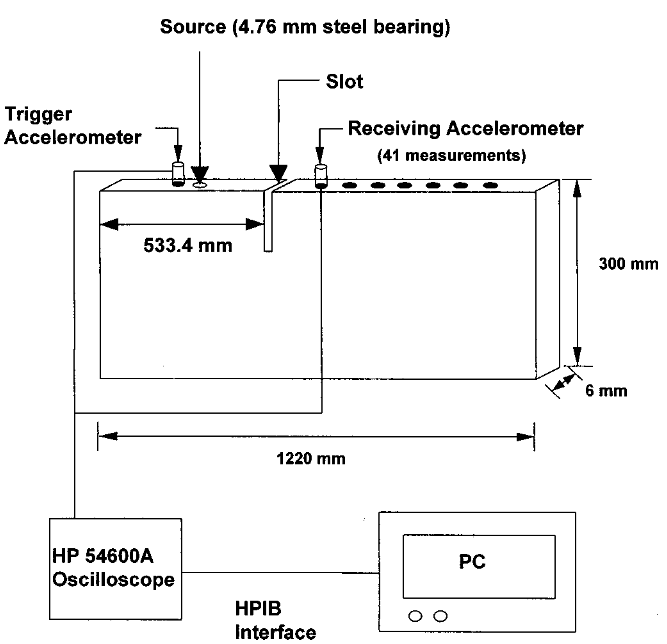

Fig. 2. Experimental setup for test series I

Theory and Background

The Rayleigh-Lamb frequency equation governs the propagation of Rayleigh waves in thin plates (Rayleigh 1888; Lamb 1889)

$$\frac{\tan\beta b}{\tan\alpha b}+\left\{\frac{4\alpha\beta k^2}{(k^2-\beta^2)}\right\}^{\pm 1}=0 \tag{1}$$

where

$$\alpha^2=\frac{\omega^2}{V_P^2}-k^2, \qquad \beta^2=\frac{\omega^2}{V_S^2}-k^2$$

and b = half the plate thickness; ω = circular frequency; k = wave number; and the compressional and shear wave velocities in the three-dimensional space are given by V_P and V_S, respectively. An exponent of $+1$ gives the symmetric components, whereas an exponent of -1 provides the antisymmetric components. In sub-

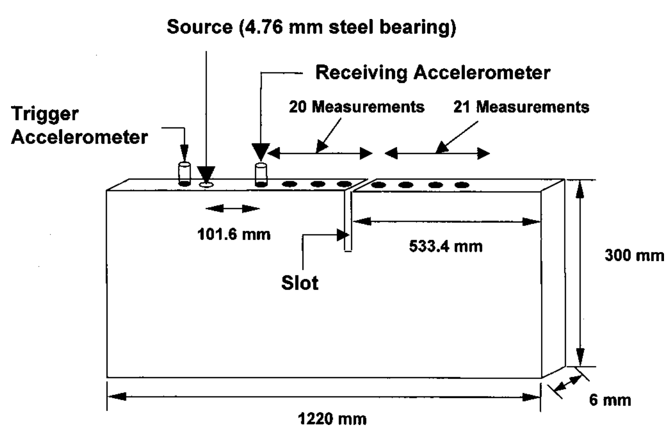

Fig. 3. Experimental setup for test series II

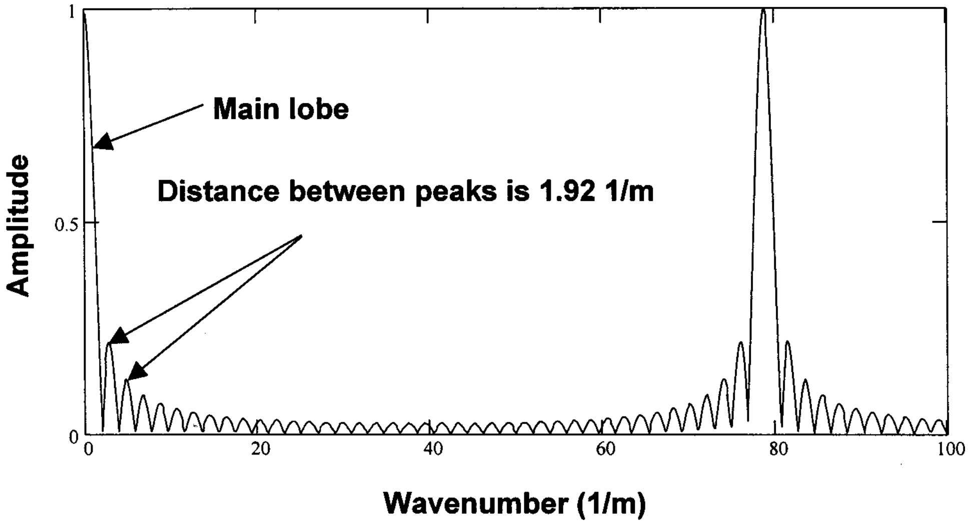

Fig. 4. Aperture function for an array with 41 receivers spaced 12.7 mm apart

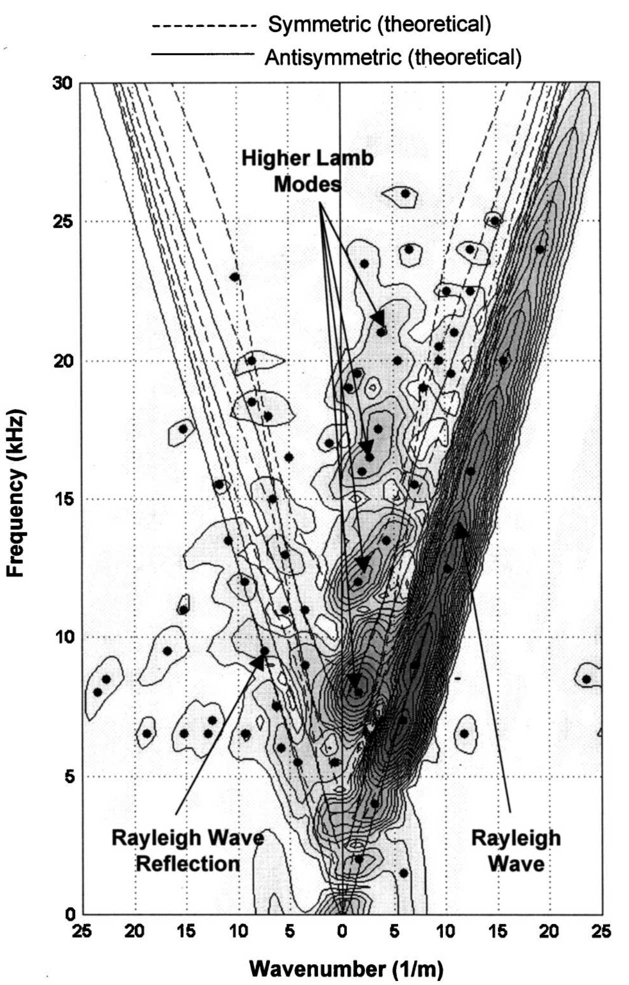

Fig. 5. Frequency–wave-number plot for measurements without slot; dashed lines represent symmetric Lamb modes and solid lines denote antisymmetric Lamb modes

sequent plots, symmetric modes are plotted with a dashed line, and a solid line is used for antisymmetric modes.

Rayleigh waves in a plate are formed by the superposition of fundamental symmetric (S_0) and antisymmetric (A_0) Lamb modes (Victorov 1967). Dispersion curves for the fundamental Lamb modes are shown in Fig. 1. These curves are calculated

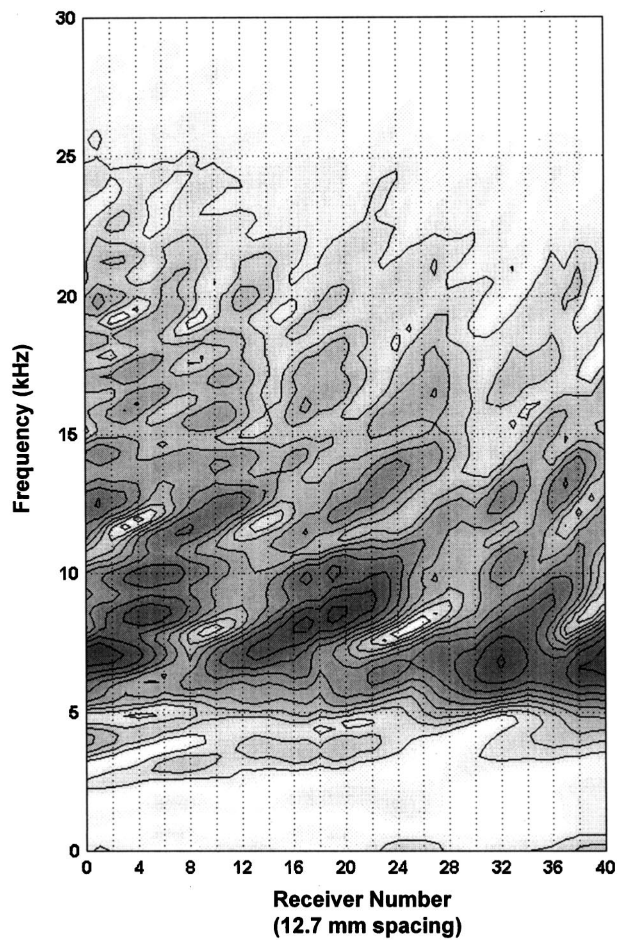

Fig. 6. Autospectrum calculations for measurements without slot

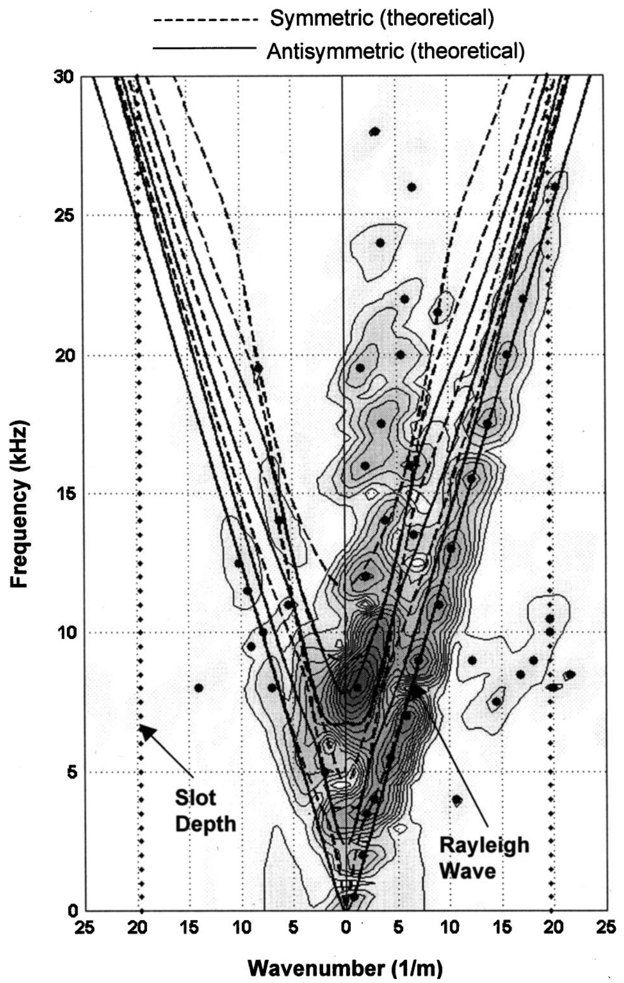

Fig. 7. Frequency–wave-number plot for 50.8 mm slot; theoretical Lamb mode dispersion curves are superimposed

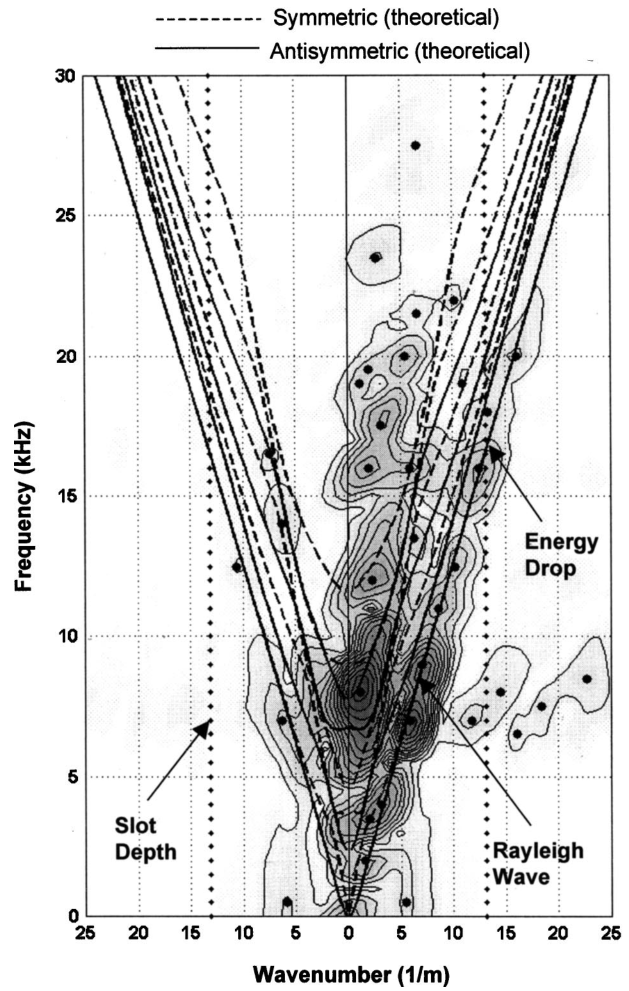

Fig. 8. Frequency–wave-number plot for 76.2 mm slot; theoretical Lamb mode dispersion curves are superimposed

using Eq. (1) and a half-plate thickness of 152.4 mm with compression and shear wave velocities of 2,370 and 1,370 m/s, respectively. The three-dimensional (3D) compression wave velocity in Plexiglas is 2,700 m/s; however, generalized plane stress conditions which prevail through the plate width reduce the compression wave velocity to 2,370 m/s (Zerwer et al. 2000). Fig. 1 shows that the phase velocity of the fundamental modes approaches the Rayleigh wave velocity as the frequency increases, illustrating that Rayleigh waves form at wavelengths shorter than half the plate thickness and that fundamental Lamb mode behavior occurs at longer wavelengths.

Experimental Study: Description and Measurement Configuration

The experimental approach is to model the geometry of a typical beam or column by using a thin plate to represent a ''slice'' of a rectangular member. In this way, two-dimensional wave propagation (generalized plane stress condition) prevails in a plate held in an upright position (Figs. 2 and 3). Plexiglas is the material used in these experiments to simplify the material parameters so that the main focus is on the geometric implications of Rayleigh wave propagation. The test configuration is as follows.

A sheet of Plexiglas with dimensions $1{,}220\times300\times6\ \mathrm{mm}^3$ is maintained in an upright position. The source for these measurements is a 4.74 mm (3/16 in.) steel bearing, dropped onto the edge of a Plexiglas sheet. A glass tube with a length of 50 mm guides the steel bearing. An accelerometer coupled to the plate by a thin layer of beeswax measures the vertical component of acceleration at different locations on the Plexiglas sheet. Time series are captured with a digital oscilloscope and stored in a computer for analysis. A second accelerometer, mounted 3 mm behind the source, acts as a trigger.

Two measurement configurations are implemented to study the Rayleigh wave/fracture interaction for various slot depths and receiver array locations. These are schematically shown in Figs. 2 and 3. The intent is to examine wavefronts before and after the slot.

Test Series I (array opposite the slot). For these experiments, the source is placed 101.6 mm (4 in.), 203.2 mm (8 in.), and 304.8 mm (12 in.) in front of the slot. All 41 receiver measurements are made on the opposite side of the slot, with the first measurement located 25.4 mm (1 in.) behind the slot. Initial measurements are done without a slot, and in subsequent measurements the slot depth is increased at 25.4-mm (1 in.) intervals up to 152.4 mm (6 in.). The experimental setup for these tests is shown in Fig. 2.

Test Series II (array straddling the slot). In these experiments, 20 receiver measurements are made in front of the slot and 21 are made behind the slot, as shown in Fig. 3. The source is located 101.6 mm (4 in.) from the first receiver.

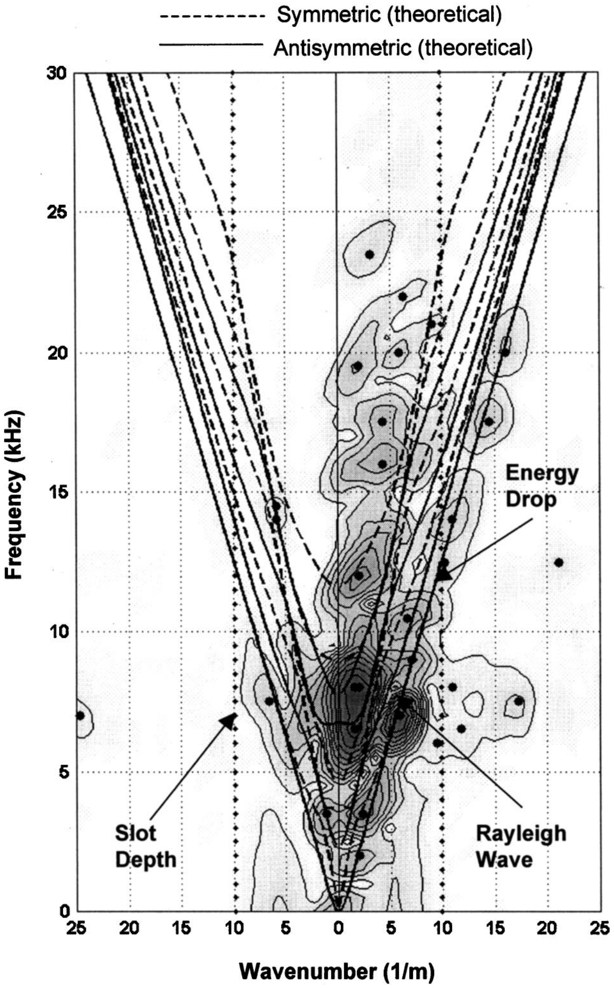

Fig. 9. Frequency–wave-number plot for 101.6 mm slot; theoretical Lamb mode dispersion curves are superimposed

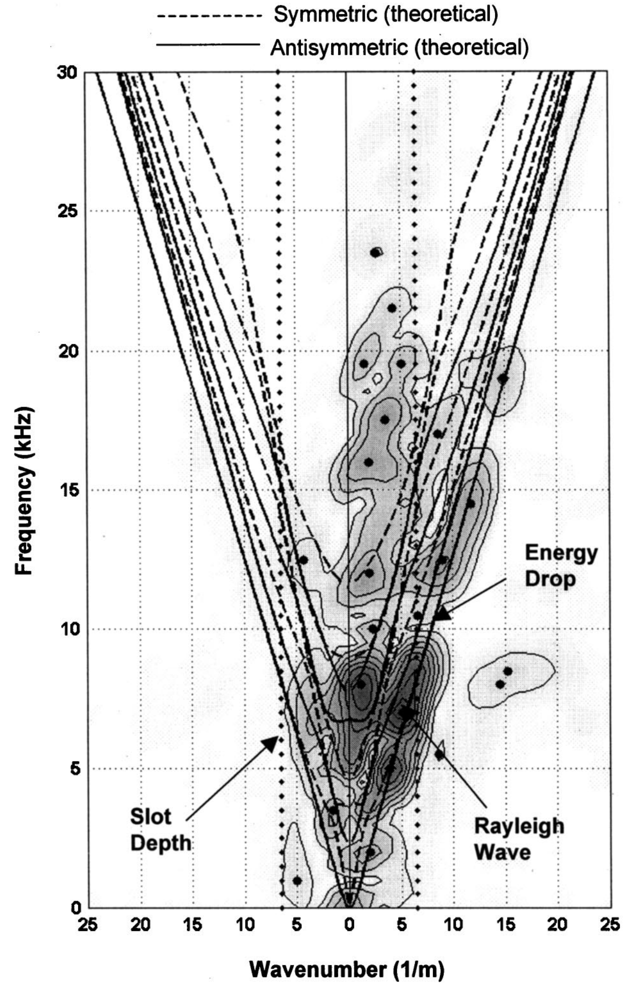

Fig. 10. Frequency–wave-number plot for 152.4 mm slot; theoretical Lamb mode dispersion curves are superimposed

Signal Processing

Two signal-processing techniques are applied to the collected data to enhance interpretation. First, a two-dimensional Fourier transform converts the array of time-history measurements into the frequency–wave-number domain. Second, the autospectral density is computed for each signal to reveal changes in energy content along the array.

The steel-bearing source used in these measurements produces a broadband signal which can excite many vibrational modes at once. To distinguish the various modes, in particular the Rayleigh wave, an equidistant number of receiver measurements are recorded and transformed into the frequency–wave-number domain using a two-dimensional Fourier transform (Alleyne and Cawley 1991; Costley and Berthelot 1994; Zerwer et al. 1999). The equidistant time-history measurements are assembled into a matrix where the columns represent amplitudes in time and rows correspond to amplitudes in space. The two-dimensional Fourier transform is

$$X(\omega,k)=\sum_{n=-\infty}^{\infty}\sum_{m=-\infty}^{\infty}x(n\Delta t,m\Delta x)e^{-i[\omega(n\Delta t)-k(m\Delta x)]} \quad (2)$$

where k = wave number and f = frequency. The numerical implementation involves applying a one-dimensional Fourier transform to both rows and columns of the assembled matrix. A hamming window function is applied to the assembled time-space matrix to prevent leakage in the frequency–wave-number domain. Magnitude values are calculated for each element of the transformed matrix, and are graphed as a contour plot. Peaks in the contour plot permit computing the phase velocities for measured active modes. Also, the contours provide a relative measure of energy and can be used to gauge mode participation.

An important property of the two-dimensional Fourier transform is rotational invariance (Peardon 1984). Lines joining arrivals in the time-space domain are rotated $+90°$ (counterclockwise) in the frequency–wave-number domain. Therefore, waves propagating either left to right or vice versa through the array can be distinguished. In the following, frequency–wave-number plot contours to the right of $k=0$ represent waves moving left-right (direct wave) through the array, and those to the left of $k=0$ correspond to waves moving right-left (reflected wave) along the array.

The autospectral density is the spectrum of energy content in a signal. To calculate autospectral densities, the signal is transformed into the frequency domain, followed by squaring the resulting Fourier components (Santamarina and Fratta 1998)

$$X=\mathrm{DFT}(x) \quad (3)$$

$$\mathrm{Autocorrelation}=X^{*}\mathrm{X} \quad (4)$$

$$\mathrm{Autospectral\ Density}=[\mathrm{Re}(X)]^2+[\mathrm{Im}(\mathrm{X})]^2 \quad (5)$$

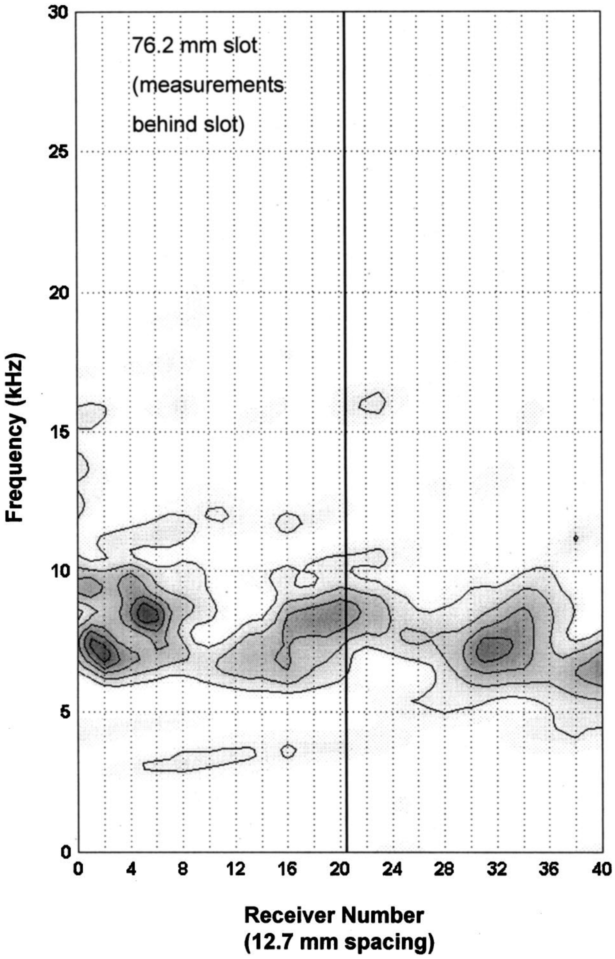

Fig. 11. Autospectrum calculations for 76.2 mm slot; measurements made behind slot

where DFT = discrete Fourier transform and the bar represents complex conjugate. Results are presented as autospectral density versus receiver location (Cascante et al. 1999).

Aperture Function

The resolution of the receiver array measurement is defined by the aperture function. A series of receiver measurements made along a straight line can be considered as a one-dimensional array. Distances between receiver measurements defines the sampling interval in the spatial domain. The aperture function indicates the resolution of an array, which in this study is entirely defined by the receiver spacing (Johnson and Dudgeon 1993). For the one-dimensional case, the aperture function (AF) is defined as

$$\mathrm{AF}(k)=\frac{1}{N}\sum_{i=0}^{N-1} w_i e^{-ikx_i} \tag{6}$$

where N = number of receivers, w_i = weighting of each receiver measurement, and x_i = receiver location. Assuming equal weights for all receivers ($w_i=1$), the analytical solution of the aperture function becomes

$$\mathrm{AF}(k)=\frac{\sin\left(Nk\dfrac{D}{2}\right)}{N\sin\left(k\dfrac{D}{2}\right)}e^{-i[(N-1)kD/2]} \tag{7}$$

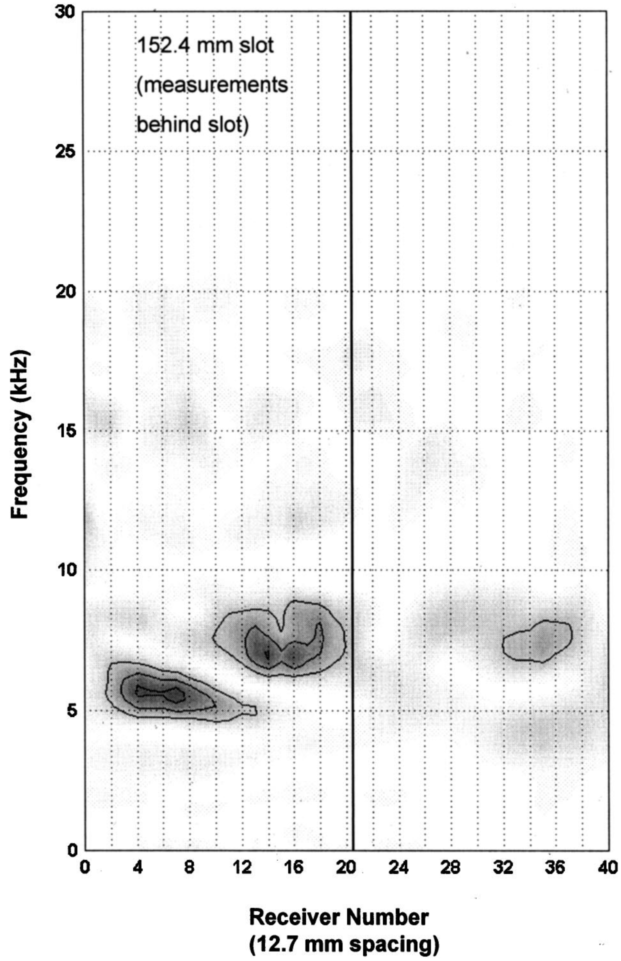

Fig. 12. Autospectrum calculations for 152.4 mm slot; measurements made behind slot

where D = distance between receivers.

In this study, 41 receiver measurements are made at a spacing of 12.7 mm. The computed aperture function is shown in Fig. 4. This figure shows the main lobe followed by a series of sidelobes. The spacing between peaks in Fig. 4 is 1.92 m^{-1}, which also defines the spacing between peaks in the frequency–wave-number plots. Spatial aliasing begins at the second mainlobe.

Measurement Results

Measurements Without a Slot

The measurement made using the 101.6 mm (4 in.) source distance, following the configuration used in test series I, serves as the reference case for the measurement without a slot. Measured dispersion and autospectral densities are shown in Figs. 5 and 6. The Rayleigh wave is observed at frequencies between 2.5 and 30 kHz (Fig. 5). The phase velocity is constant within this frequency range. Higher Lamb modes are also observed. Cutoff frequencies for the higher Lamb modes appear at 7.5, 12, 16, and 19.5 kHz. Dispersion curves are calculated up to the fourth symmetric mode; however, not all of the symmetric and antisymmetric modes are observed in the frequency–wave-number plots. Briefly, the magnitude of vertical accelerations recorded along the edge of the plate is dependent on the mode shape of the propagating mode. Some modes exhibit low-amplitude motions near the surface, whereas other modes have strong surface motions (i.e., the Rayleigh wave). In addition, the frequency characteristics of the

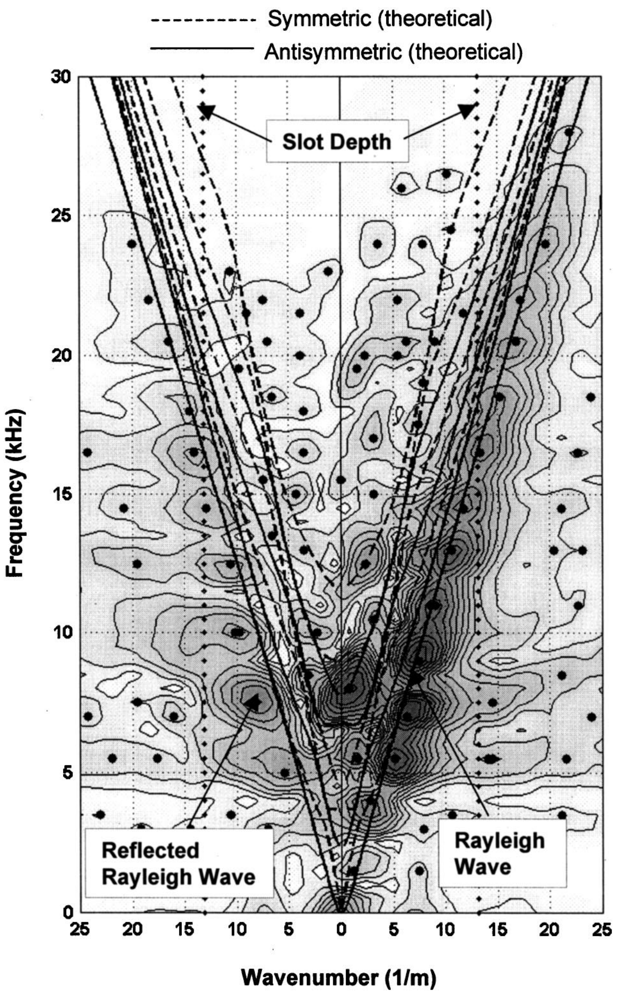

Fig. 13. Frequency–wave-number plot for measurements of 76.2 mm slot; slot in middle of receiver array

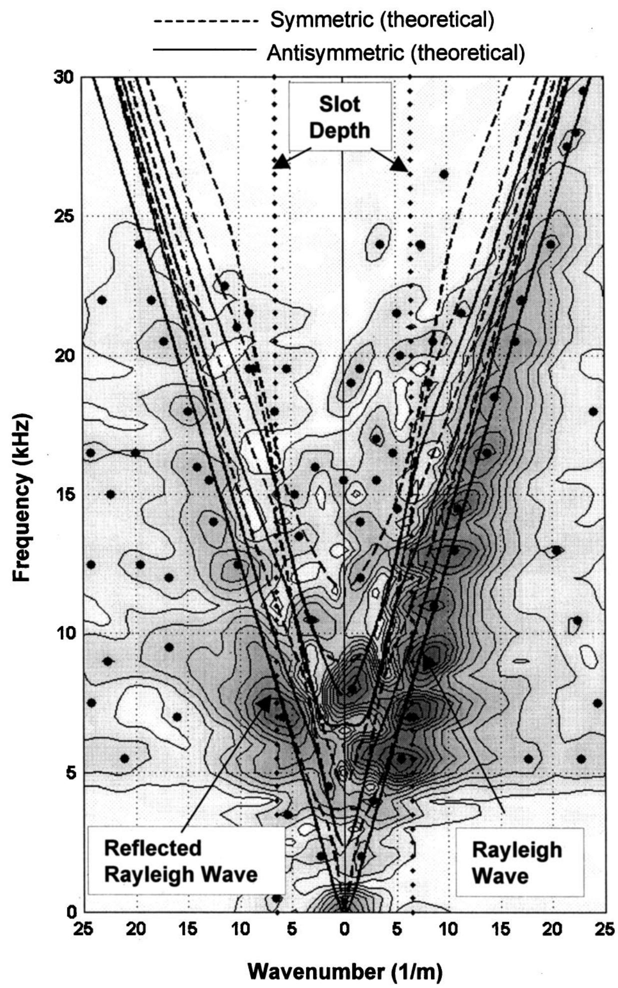

Fig. 14. Frequency–wave-number plot for measurements of 152.4 mm slot; slot in middle of receiver array

source dictate which modes are activated, resulting in discrete dispersion curves (Lange and Bottega 1998). Because of the difficulty in relating active modes to a source for different geometries (i.e., rectangular plates), the measured results are compared with continuous dispersion curves calculated using the Rayleigh-Lamb frequency equations.

The energy related to the Rayleigh wave is not clearly defined in the autospectral density plot of Fig. 6. Low-frequency, high-amplitude peaks can be attributed to the Rayleigh wave motion, however multiple reflections of width and thickness in the Lamb modes add complexity to the autospectral density measurements. Identifying energy components related to specific modes cannot be reliably done in this space. Nevertheless, autospectral density measurements are useful in determining regions of strong energy changes, such as the presence of a fracture or a slot.

Test Series I

Dispersion plots are shown in Figs. 7–10 for the 50.8, 76.2, 101.6, and 154.2 mm slot depths. For measurements with a slot, the frequency-wavenumber plots have a vertical dotted line that corresponds to the slot depth at a position of $K=1/h$ (where h is the slot depth). As the slot depth increases, the energy of the Rayleigh wave decreases for all frequencies and wave numbers. A decrease in the main energy band of the Rayleigh wave is observed for 50.8 mm slot. For the 76.2 and 101.6 mm slots, a distinct drop is recorded in the main energy band of the Rayleigh wave associated with the slot depth. The location of the energy reduction is less apparent for the 127 and 152.4 mm slot depths, however the energy drop is more pronounced when the source distance is increased. In all cases, some Rayleigh wave energy is found at wavelengths shorter than the slot depth. Also, weak Rayleigh wave reflections from the end of the plate are measured to the left of $k=0$. The energy of the Rayleigh wave reflections remains almost unchanged as the slot depth increases.

The autospectrum calculations show a similar response to the frequency–wave-number results. As the slot depth increases, high-frequency components are not present in the spectrum. However, the high-frequency cutoff does not correspond well with the slot depth, as shown in Figs. 11 and 12. The main difficulty in calculating a wavelength for a peak in the autospectrum plot is not knowing to which propagation mode the peak belongs. Overall, the energy decreases for all frequencies with increasing slot depth. This result is expected because a deeper slot will allow less energy to move past the slot.

Test Series II

The frequency–wave-number plot for the measurement without a slot is shown in Fig. 5. The Rayleigh wave and higher Lamb

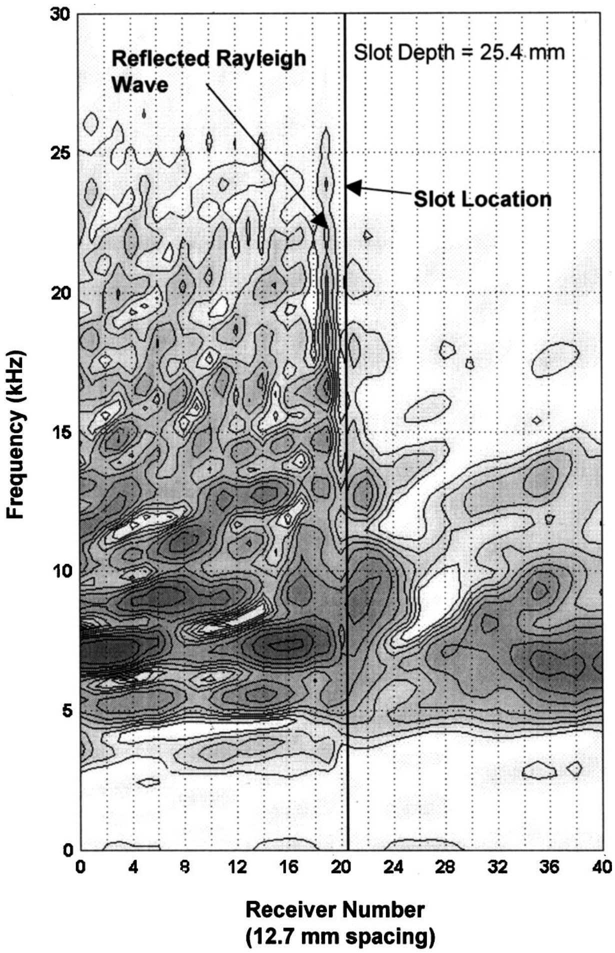

Fig. 15. Autospectrum calculations for 25.4 mm slot; slot in middle of receiver array

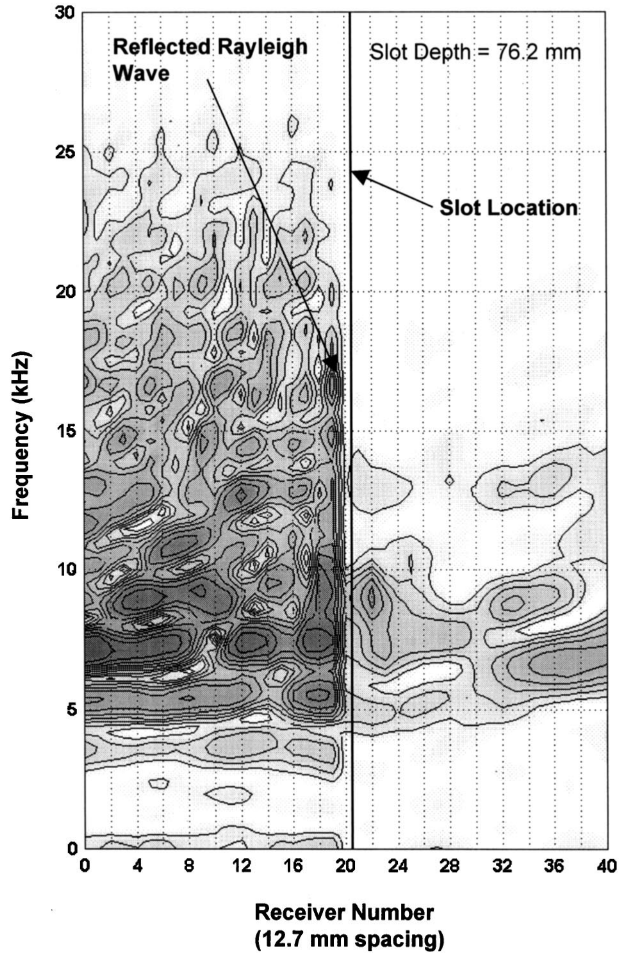

Fig. 16. Autospectrum calculations for 76.2 mm slot; slot in middle of receiver array

modes are visible and no energy is observed traveling right to left through the receiver array, i.e., no reflections. As the slot depth increases, the width of the main energy band of the Rayleigh wave increases, a result of fewer receivers measuring a strong Rayleigh wave. In addition, the reflections from the front of the slot are visible at wavenumbers to the left of $k=0$. Figs. 13 and 14 show the frequency–wave-number plot obtained from a 76.2 and 152.4 mm slot. A clear definition of slot depth and location cannot be gained from these measurements, however the presence of the slot is apparent.

The autospectral density versus distance plot clearly defines the slot location (where high-frequency energy vanishes) and gives an indication of slot depth (from the cutoff frequency). Autospectrum calculations without a slot are similar to Fig. 6. Results for the 25.4, 76.2, and 152.4 mm slot depths are shown in Figs. 15–17. The strong signal is a Rayleigh wave reflected from the slot. The vertical distribution of Rayleigh wave energy suggests that the Rayleigh wave is unaffected by the reflections from other propagating modes.

Conclusions: Implications for Fracture Detection

The purpose of this study is to assess the potential for detection and sizing of surface discontinuities with Rayleigh waves. The experimental study involves 2D physical models, arrays of sensors, and signal processing. Frequency–wave-number plots show the transmission of longer wavelengths past the slot ($\lambda/d>1$) and the reflection of shorter wavelengths ($\lambda/d<1$). Energy drops are easier to identify for deeper slots; however, determining the exact slot depths from the frequency–wave-number plots becomes more difficult.

The main reason for inaccuracies in depth determination for deep slots is the spatial resolution of the array. A discrete receiver spacing acts inherently as a filter. This effect is similar to the filtering effects of various window functions. For 41 receiver measurements, peaks in the frequency–wave-number plots are spaced apart by 1.92 m^{-1} (Fig. 4). Furthermore, in test series II only 20 receivers measure a strong Rayleigh wave, which increases the peak spacing to 3.84 m^{-1} as shown in Fig. 18(a). Additional error is introduced because wavelength is inversely proportional to wave number. Fewer data points are present at lower frequencies, as illustrated in Figs. 18(b and c).

The autospectrum calculations show strong reflections allowing easy identification of slot location. Autospectral density plots also provide a relative indication of slot depth.

Observations from these measurements provide insight into practical application of this methodology for nondestructive testing. The best detection strategy is to combine a series of array measurements. The initial step is to calculate the autospectrum for all receiver measurements to define locations where cracks may exist. Receiver measurements made behind the fracture can be used subsequently to calculate frequency–wave-number plots to determine fracture depths.

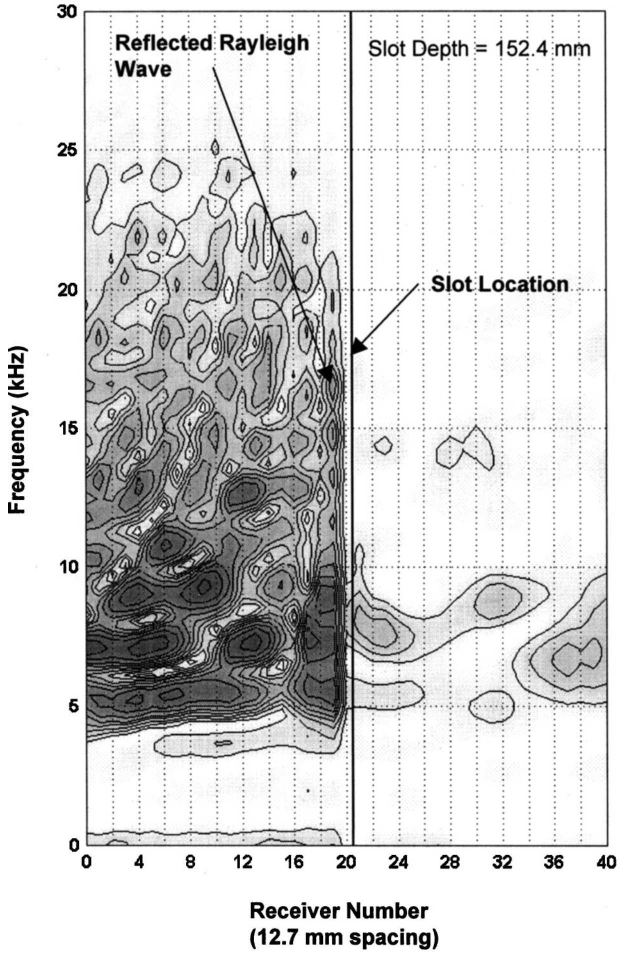

Fig. 17. Autospectrum calculations for 152.4 mm slot; slot in middle of receiver array

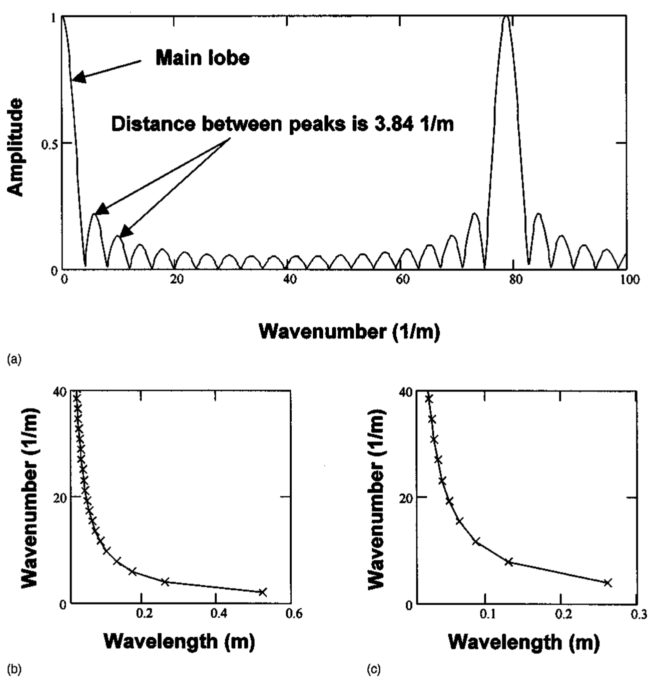

Fig. 18. (a) Aperture function for 20 receivers spaced 12.7 mm apart; (b) resolution for 41 receiver measurements; (c) resolution for 20 receiver measurements

Acknowledgments

The presented research was supported by the Natural Sciences and Engineering Research Council of Canada (NSERC) and MDC Geological Consultants. The writers wish to express their appreciation for the support.

References

Alleyne, D., and Cawley, P. (1991). ‘‘A two-dimensional Fourier transform method for the measurement of propagating multimode signals.’’ *J. Acoust. Soc. Am.*, 89(3), 1159–1168.

Cascante, G., Hutchinson, J., and Phillips, C. (1999) ‘‘Assessment of the spectral analysis of surface waves method for detecting underground voids.’’ *Proc., 52nd Canadian Geotechnical Conf.*, Canadian Geotechnical Society, Toronto, 49–53.

Costley, R. D., Jr., and Berthelot, Y. H. (1994). ‘‘Dispersion curve analysis of laser-generated Lamb waves.’’ *Ultrasonics*, 32(4), 249–253.

Domarkus, V., Khuri-Yakub, B. T., and Kino, G. S. (1978). ‘‘Length and depth resonances of surface cracks and their use for crack-size estimation.’’ *Appl. Phys. Lett.*, 33(7), 557–559.

Hévin, G., Abraham, O., Pedersen, H. A., and Campillo, M. (1998). ‘‘Characterisation of surface cracks with Rayleigh waves: A numerical model.’’ *NDT&E Int.*, 31(4), 289–297.

Hirao, M., Tojo, K., and Fukuoka, H. (1992). ‘‘Spectrum analysis for Rayleigh waves reflected from small fatigue cracks.’’ *Nondestr. Test. Eval.*, 7, 223–232.

Johnson, D. H., and Dudgeon, D. E. (1993). *Array signal processing: Concepts and techniques*, Prentice Hall, Englewood Cliffs, N.J.

Lamb, H. (1889). ‘‘On waves in an elastic plate.’’ *Proc. London Math. Soc.*, 21, 85–95.

Lange, K. A., and Bottega, W. J. (1998). ‘‘On the elastodynamic response of thick multilayered plates subjected to impact loads.’’ *J. Sound Vib.*, 211(1), 39–93.

Pant, D. R., and Greenhalgh, S. A. (1989). ‘‘Blocking surface wave by a cut: Physical seismic model results.’’ *Geophys. Prospect.*, 37, 589–605.

Peardon, L. G. (1986). ‘‘FK techniques in seismic processing.’’ *Geophysical signal processing*, Prentice-Hall, Englewood Cliffs, N.J., 388–474.

Rayleigh, L. (1888). ‘‘On waves propagated along the plane surface of an elastic solid.’’ *Proc. London Math. Soc.*, 17, 4–11.

Santamarina, J. C., and Fratta, D. (1998). *Introduction to signal and inverse problems in civil engineering*, ASCE, N.Y.

Silk, M. G. (1976). ‘‘The determination of crack penetration using ultrasonic surface waves.’’ *Ultrasonics*, 38, 290–297.

Tittmann, B. R., et al. (1980). ‘‘Surface wave scattering from elliptical cracks for failure prediction.’’ *J. Appl. Phys.*, 51(1), 142–150.

Tittmann, B. R., Cohen-Ténouodji, F., De Billy, M., Jungman, A., and Quentin, G. (1978). ‘‘A simple approach to estimate the size of small surface cracks with the use of acoustic surface waves.’’ *Appl. Phys. Lett.*, 33(1), 6–8.

Victorov, I. (1967). *Rayleigh and Lamb waves: Physical theory and applications*, Plenum, New York.

Woods, R. D. (1968). ‘‘Screening of surface waves in soils.’’ *J. Soil Mech. Found. Div., Am. Soc. Civil Eng.*, 94(SM4), 951–979.

Yew, C. H., Chen, K. G., and Wang, D. L. (1984). ‘‘An experimental study of interaction between surface waves and surface breaking crack.’’ *J. Acoust. Soc. Am.*, 75(1), 189–196.

Zerwer, A. (1999). ‘‘Near surface fracture detection in structural elements: Investigation using Rayleigh waves.’’ PhD Dissertation, Dept. of Civil Engineering, Univ. of Waterloo.

Zerwer, A., Polak, M. A., and Santamarina, J. C. (2000). ‘‘Wave propagation in thin Plexiglas plates: Implications for Rayleigh waves.’’ *NDT&E Int.*, 33, 33–41.